

Disruption of Alfvénic turbulence by magnetic reconnection in a collisionless plasma

Alfred Mallet^{1†}, A. A. Schekochihin^{2,3} and B. D. G. Chandran¹

¹Space Science Center, University of New Hampshire, Durham, NH 03824, USA

²Rudolf Peierls Centre for Theoretical Physics, University of Oxford, Oxford OX1 3NP, UK

³Merton College, Oxford OX1 4JD, UK

(Received xx; revised xx; accepted xx)

We calculate the disruption scale λ_D at which sheet-like structures in dynamically aligned Alfvénic turbulence are destroyed by the onset of magnetic reconnection in a low- β collisionless plasma. The scaling of λ_D depends on the order of the statistics being considered, with more intense structures being disrupted at larger scales. The disruption scale for the structures that dominate the energy spectrum is $\lambda_D \sim L_\perp^{1/9} (d_e \rho_s)^{4/9}$, where d_e is the electron inertial scale, ρ_s is the ion sound scale, and L_\perp is the outer scale of the turbulence. When β_e and ρ_s/L_\perp are sufficiently small, the scale λ_D is larger than ρ_s and there is a break in the energy spectrum at λ_D , rather than at ρ_s . We propose that the fluctuations produced by the disruption are circularised flux ropes, which may have already been observed in the solar wind. We predict the relationship between the amplitude and radius of these structures and quantify the importance of the disruption process to the cascade in terms of the filling fraction of undisrupted structures and the fractional reduction of the energy contained in them at the ion sound scale ρ_s . Both of these fractions depend strongly on β_e , with the disrupted structures becoming more important at lower β_e . Finally, we predict that the energy spectrum between λ_D and ρ_s is steeper than k_\perp^{-3} , when this range exists. Such a steep “transition range” is sometimes observed in short intervals of solar-wind turbulence. The onset of collisionless magnetic reconnection may therefore significantly affect the nature of plasma turbulence around the ion gyroscale.

1. Introduction

Astrophysical plasmas are often turbulent, with power-law spectra over a wide range of scales. In many situations, a strong background magnetic field \mathbf{B}_0 can be assumed, and often the plasma is only weakly collisional. A well-studied example of such a system is the solar wind, in which the turbulence is directly measured by spacecraft (Bruno & Carbone 2013; Chen 2016). The nature of the turbulence depends on how the scale of interest compares to the ion gyroradius $\rho_i = v_{thi}/\Omega_i$, where the ion thermal speed $v_{thi} = \sqrt{2T_i/m_i}$ and the ion gyrofrequency $\Omega_i = ZeB_0/m_i c$. Regardless of whether the plasma is collisional or collisionless, on length scales much larger than the ion gyroradius, $k_\perp \rho_i \ll 1$, Alfvénically polarized fluctuations obey the RMHD equations (Kadomtsev & Pogutse 1973; Strauss 1976; Schekochihin *et al.* 2009), which describe nonlinearly interacting Alfvén wavepackets (represented by the Elsasser fields $\mathbf{z}_\pm^\pm = \mathbf{u} \pm \mathbf{b}$) propagating up and down the background magnetic field at the Alfvén speed

† Email address for correspondence: alfred.mallet@unh.edu

$v_A = B_0/\sqrt{4\pi m_i n_i}$. At smaller, “kinetic” scales, $k_\perp \rho_i \gtrsim 1$, the Alfvén waves become dispersive “kinetic Alfvén waves” (as confirmed in the solar wind: see Chen *et al.* 2013).

The structure of strong RMHD turbulence at large scales, $k_\perp \rho_i \ll 1$, is relatively well understood. First, the fluctuations are “critically balanced” (Goldreich & Sridhar 1995, 1997; Mallet *et al.* 2015) – their linear timescale $\tau_A \sim l_\parallel/v_A$ and nonlinear timescale τ_{nl} are comparable (here l_\parallel is the parallel coherence length). This leads to anisotropic fluctuations with $l_\parallel \gg \lambda$, where $\lambda \sim 1/k_\perp$ is the perpendicular coherence scale. Second, at least in numerical simulations (Mason *et al.* 2006; Perez *et al.* 2012), the fluctuations dynamically “align” so that the vector velocity and magnetic-field perturbations point in the same direction up to a small, scale-dependent angle θ (Boldyrev 2006; Chandran *et al.* 2015; Mallet & Schekochihin 2017). This causes the fluctuations to become anisotropic within the perpendicular plane, with scale $\xi \gg \lambda$ in the direction of the vector-field perturbations. Together, these two phenomena mean that the turbulent structures are 3D anisotropic, with $l_\parallel \gg \xi \gg \lambda$. This anisotropy has been measured both in numerical simulations (Verdini & Grappin 2015; Mallet *et al.* 2016) and in the solar wind (Chen *et al.* 2012), and results in the turbulent structures becoming increasingly sheet-like at smaller scales. We review scalings obtained in a simple model of this type of Alfvénic turbulence by Mallet & Schekochihin (2017) in Section 2. At smaller scales $\lambda \lesssim \rho_i$, the turbulence is also likely to be critically balanced (Cho & Lazarian 2004; Schekochihin *et al.* 2009; Boldyrev & Perez 2012; TenBarge & Howes 2012) and has a steeper perpendicular spectral index of approximately -2.8 (Alexandrova *et al.* 2009; Chen *et al.* 2010; Sahraoui *et al.* 2010).

Since sheet-like structures are generically unstable to the tearing mode and the onset of magnetic reconnection, the formation of such structures by the large-scale Alfvénic turbulence immediately suggests that at some scale, the reconnection process may become faster than the dynamically aligning cascade, and disrupt the sheet-like structures. In resistive RMHD, the disruption scale was calculated by Mallet *et al.* (2017) and Loureiro & Boldyrev (2017a) as $\lambda_D \sim L_\perp S_{L_\perp}^{-4/7}$, where $S_{L_\perp} \doteq L_\perp \overline{\delta z}/\eta$ is the outer-scale Lundquist number (equivalently, the magnetic Reynolds number), η being the Ohmic diffusivity (resistivity). At scale λ_D , the sheet-like structures reconnect, and are converted into circularised flux ropes with radius λ_D , destroying the dynamic alignment. Below λ_D , Mallet *et al.* (2017) proposed that these flux-rope-like structures realign and are disrupted again in a recursive fashion, leading to a steeper spectrum of approximately $k_\perp^{-11/5}$ and a final dissipative cutoff scale of $\lambda_\eta \sim L_\perp S_{L_\perp}^{-3/4}$ †. This quantifies the role that reconnection plays in the dynamics of MHD turbulence, a topic that has a long history (Matthaeus & Lamkin 1986; Politano *et al.* 1989; Retinò *et al.* 2007; Sundkvist *et al.* 2007; Servidio *et al.* 2009; Zhdankin *et al.* 2013; Osman *et al.* 2014; Greco *et al.* 2016; Cerri & Califano 2017; Cerri *et al.* 2017; Franci *et al.* 2017).

Here, we extend the Mallet *et al.* (2017) model of the disruption of Alfvénic turbulence by reconnection to the low- β_e collisionless case, where the reconnection is enabled by electron inertia, rather than resistivity. The nature of the tearing mode in this regime is reviewed in Section 3. Our main conclusion, arrived at in Section 4, is that for sufficiently low electron beta $\beta_e = 8\pi n_e T_e/B_0^2$ and large enough separation between the ion sound scale $\rho_s = \rho_i \sqrt{Z T_e/2 T_i} \sim \rho_i$ (**we are assuming that $T_e \sim T_i$**) and the outer scale L_\perp , the onset of reconnection may cause the turbulence to be disrupted, inducing a spectral break at a scale λ_D larger than the scale $\sqrt{\rho_i^2/2 + \rho_s^2} \sim \rho_i \sim \rho_s$ at which the Alfvén waves in this regime become dispersive (Zocco & Schekochihin 2011). This means

† Boldyrev & Loureiro (2017) agree with these scalings of the spectrum and the dissipative cutoff but do not believe that tearing-produced islands can fully circularize.

that the turbulent structures around the ion scale, which are the starting point for the kinetic-Alfvén-wave turbulent cascade at smaller scales, are created by tearing-induced disruption of the large-scale sheets produced by the RMHD turbulent dynamics, rather than solely by the change in the dispersion relation governing the linear wave response (cf. Cerri & Califano 2017; Franci *et al.* 2017).

In the solar wind at 1AU, where $\beta_e \sim 1$, we predict that only the most intense sheet-like structures are disrupted and converted into flux ropes. Interestingly, “Alfvén vortices”, which appear to be very similar to the flux-rope structures, have already been observed even in the solar wind at 1AU (Lion *et al.* 2016; Perrone *et al.* 2016). The mechanism proposed in this paper is a physical way to generate these structures. In Section 5, we derive the fractional reduction in the volume filled by and energy contained within undisrupted, sheet-like structures at the ion sound scale as a function of β_e , showing that both these fractions decrease as β_e decreases. We also derive the dependence of the amplitude of the newly formed flux ropes on their scale – this could be compared with the observed Alfvén vortices. Closer to the Sun, in the region to be explored by the Parker Solar Probe (Fox *et al.* 2016), it is expected that, at least in fast-solar-wind streams, $\beta_e \approx 0.01$ (Chandran *et al.* 2011), in which case the moderate-amplitude structures that dominate the energy spectrum may be disrupted. Thus, our results may be especially relevant to the turbulence that will be observed by this new mission. In Section 6, we derive approximate scalings for the energy spectrum in the (very narrow) range between λ_D and ρ_s , and show that it is somewhat steeper than -3 . In the Appendix, we derive the disruption scale and the scalings for the energy spectrum in the “semicollisional” case, where the reconnection is enabled by resistivity, but the diffusion layer is much thinner than the ion scale ρ_s – a situation that is relevant to many laboratory experiments, e.g., TREX (Forest *et al.* 2015) and FLARE (Ji *et al.* 2014), as well as in hybrid kinetic simulations (e.g., Parashar *et al.* 2009; Kunz *et al.* 2014; Cerri & Califano 2017; Cerri *et al.* 2017).

2. Alfvénic turbulence model

In the theory of intermittent Alfvénic turbulence of Mallet & Schekochihin (2017), the turbulence is modelled as an ensemble of structures, each of which is characterised by an Elsasser amplitude δz and three characteristic scales: l_{\parallel} (parallel), λ (perpendicular) and ξ (fluctuation-direction). We normalise these variables by their values at the outer scale:

$$\delta \hat{z} = \frac{\delta z}{\overline{\delta z}}, \quad \hat{\lambda} = \frac{\lambda}{L_{\perp}}, \quad \hat{l}_{\parallel} = \frac{l_{\parallel}}{L_{\parallel}}, \quad \hat{\xi} = \frac{\xi}{L_{\perp}}, \quad (2.1)$$

where $\overline{\delta z}$ is the outer-scale fluctuation amplitude, and L_{\perp} and L_{\parallel} are the perpendicular and parallel outer scales. In the following, we will treat $\hat{\lambda}$ as a parameter (i.e. we are conditioning on $\hat{\lambda}$): the distribution of $\delta \hat{z}$ depends on $\hat{\lambda}$, and $\hat{\xi}$ and \hat{l}_{\parallel} are calculated from $\delta \hat{z}$ and $\hat{\lambda}$. It is assumed that the turbulence is critically balanced already at the outer scale. The normalised amplitude is given by

$$\delta \hat{z} \sim A^q, \quad (2.2)$$

where q is a Poisson-distributed random variable,

$$P(q) = \frac{\mu^q}{q!} e^{-\mu}, \quad (2.3)$$

with mean $\mu = -\ln \hat{\lambda}^\dagger$ and $\Lambda = 1/\sqrt{2}$ is a dimensionless constant (which Mallet & Schekochihin 2017 called β , but which we here rename to avoid confusion with β_e). The scalings of perpendicular structure functions are then given by

$$\langle \delta \hat{z}^n \rangle \sim \hat{\lambda}^{\zeta_n^\perp}, \quad \zeta_n^\perp = 1 - \Lambda^n. \quad (2.4)$$

The fluctuation-direction scale $\hat{\xi}$ is related to the amplitude via

$$\hat{\xi} \sim \hat{\lambda}^{1/2} \Lambda^q, \quad (2.5)$$

while the parallel scale depends only on $\hat{\lambda}$:

$$\hat{l}_\parallel \sim \hat{\lambda}^{1/2}. \quad (2.6)$$

Following Mallet *et al.* (2017), we define the “effective amplitude” of structures that dominate the n -th order perpendicular structure function:

$$\delta \hat{z}[n] \equiv \langle \delta \hat{z}^n \rangle^{1/n} \sim \hat{\lambda}^{\zeta_n^\perp/n}. \quad (2.7)$$

The effective amplitude $\delta \hat{z}[n]$ is a strictly increasing function of n , and so n may be used as a convenient proxy for the amplitude of the structures at a given scale. The scalings for three interesting cases can be immediately obtained from (2.7): first,

$$\delta \hat{z}[\infty] \sim 1 \quad (2.8)$$

describes the “most intense” structures, whose amplitude is independent of scale; secondly,

$$\delta \hat{z}[2] \sim \hat{\lambda}^{1/4} \quad (2.9)$$

describes the fluctuations that dominate the second-order structure function and the energy spectrum, and thus determine the spectral index; finally, the “bulk” fluctuations are described by $n \rightarrow 0$, and their amplitudes scale as

$$\delta \hat{z}[n \rightarrow 0] \sim \hat{\lambda}^{-\ln \Lambda}. \quad (2.10)$$

We will also need an expression for the (effective) fluctuation-direction scale for the n -th order fluctuations, given by

$$\hat{\xi}[n] \sim \hat{\lambda}^{1/2} \delta \hat{z}[n] \sim \hat{\lambda}^{1/2 + \zeta_n^\perp/n}, \quad (2.11)$$

and for the cascade time,

$$\tau_C \sim \frac{\xi}{\delta z} \sim \frac{L_\perp}{\delta z} \hat{\lambda}^{1/2}. \quad (2.12)$$

One can easily see from (2.11) that the structures are anisotropic in the perpendicular plane, with $\xi \gg \lambda$, and that the higher-amplitude structures are more anisotropic, consistent with numerical evidence (Mallet *et al.* 2015, 2016).

We now have all the information needed about the turbulent structures to determine whether they can be disrupted by tearing.

3. Collisionless tearing mode

Scalings for the low- β_e collisionless tearing mode are reviewed in Appendix B.3 of Zocco & Schekochihin (2011). Our sheet-like turbulent structures have a width λ and a length ξ in the perpendicular plane. We will assume that the perturbed magnetic field

[†] In the theory of Mallet & Schekochihin (2017), a slightly more complicated distribution is posited, but we ignore this nuance here and postulate (2.3).

reverses across the structure $\delta b \sim \delta z$. There is also a velocity perturbation δu associated with the δz . If the situation were that $\delta u > \delta b$, the Kelvin-Helmholtz instability would disrupt the sheets much faster than the tearing mode. However, this situation does not typically occur, because the vortex-stretching terms for the different Elsasser fields \mathbf{z}_\perp^\pm have opposite sign (Zhdankin *et al.* 2016), meaning that “current sheets” are more common than “shear layers” in RMHD turbulence, i.e., $\delta u < \delta b$ (this is also true in the solar wind; see, e.g., Chen 2016; Wicks *et al.* 2013), and the Kelvin-Helmholtz instability is naturally stabilised (Chandrasekhar 1961). For simplicity, we assume that the velocity fluctuations $\delta u \lesssim \delta b$ present in the sheet-like structures do not significantly affect the dynamics that we will describe in this paper.

The structure of the collisionless tearing mode involves three scales: the perpendicular scale λ of the turbulent structure, and a nested inner layer, where two-fluid effects become important at the ion sound scale ρ_s , while flux unfreezing happens due to electron inertia in a thinner layer controlled by the electron inertial scale $d_e = c/\omega_{pe} \ll \rho_s$, where $\omega_{pe} = \sqrt{4\pi n_e e^2/m_e}$ is the electron plasma frequency. The tearing instability’s growth rates will, therefore, involve all of these scales. The scalings that we use here will cease to apply if $\rho_s \lesssim d_e$ (i.e., $\beta_e \lesssim m_e/m_i$), at which point the ion scale becomes unimportant, and if $\beta_e \gtrsim 1$, when the flux unfreezing happens at the electron gyroradius $\rho_e = d_e \sqrt{\beta_e}$, rather than at d_e . This means that we are restricting ourselves to “moderately” small beta, $1 \gg \beta_e \gg m_e/m_i$.

We will assume a Harris-sheet-like equilibrium (Harris 1962)[†]. For long-wavelength modes ($k \ll 1/\lambda$), the instability parameter Δ' is given by

$$\Delta' \lambda \approx \frac{1}{k \lambda}. \quad (3.1)$$

For $\Delta' \delta_{\text{in}} \ll 1$, where δ_{in} is the width of the inner layer, the linear growth rate and the inner-layer width are

$$\gamma_{>} \sim k \delta z \frac{d_e \rho_s \Delta'}{\lambda} \sim \delta z \frac{d_e \rho_s}{\lambda^3}, \quad \delta_{\text{in}} \sim d_e \rho_s^{1/2} \Delta'^{1/2}. \quad (3.2)$$

For $\Delta' \delta_{\text{in}} \sim 1$, they are

$$\gamma_{<} \sim k \delta z \frac{d_e^{1/3} \rho_s^{2/3}}{\lambda}, \quad \delta_{\text{in}} \sim d_e^{2/3} \rho_s^{1/3}. \quad (3.3)$$

The wavenumber k_{tr} of the transition between these two regimes can be found by balancing the two expressions for the growth rate, giving

$$k_{\text{tr}} \sim \frac{d_e^{2/3} \rho_s^{1/3}}{\lambda^2}. \quad (3.4)$$

For $k < k_{\text{tr}}$, the growth rate is $\gamma_{<}$, while for $k > k_{\text{tr}}$, it is $\gamma_{>}$, which is independent of wavenumber. This breaks down when $k \sim 1/\lambda$, because (3.1) ceases to apply – but, since $\xi \gg \lambda$, this only happens for a very large number of islands. Therefore, the maximum growth rate is attained for all $k > k_{\text{tr}}$, and is given simply by $\gamma_{>}$. Thus there is always a mode with the maximum growth rate and a large enough wavenumber to fit into a sheet of any length $\xi > \lambda$. This is somewhat different from the resistive-RMHD case studied by Mallet *et al.* (2017), in which $\gamma_{>}^{\text{RMHD}} \propto k^{-2/5}$, while $\gamma_{<}^{\text{RMHD}} \propto k^{2/3}$, and the maximum growth rate is attained at the transitional wavenumber.

The linear-growth stage of tearing ends when the width of the islands reaches δ_{in} ,

[†] In Loureiro & Boldyrev (2017b), a more general class of equilibria is considered, which slightly affects the resulting scalings for the disruption scales and spectra.

which decreases with increasing k for $k > k_{\text{tr}}$. Thus at the end of the linear stage, the largest islands are produced by the mode with $k \sim k_{\text{tr}}$, and so, despite the independence of the linear growth rate on k , we can assume that this transitional mode dominates the nonlinear dynamics. We assume that the X -points between the islands then collapse quickly (i.e., on a timescale at most comparable to $\gamma_{>}^{-1}$), circularising the islands and forming a set of flux ropes of width λ , as appears to be consistent with numerical evidence (Loureiro *et al.* 2013). ‡ Since these structures are as wide as the original sheet, the latter should at this point be disrupted and broken up – being effectively replaced by a set of flux ropes. The scale of these ropes parallel to the (exact) magnetic field is set as usual by critical balance. Since we assume that the X -point collapse is at least as fast as the linear tearing stage, we estimate the disruption time using the linear growth rate (3.2) of the tearing mode:

$$\tau_{\text{D}} \sim \gamma_{>}^{-1}. \quad (3.5)$$

It is important to point out that the restriction to low β_e limits the applicability of our conclusions in the solar wind, where, more often than not, $\beta_e \sim 1$, but our results will be more relevant to the turbulence closer to the Sun and in the corona: indeed, at the perihelion (approximately 10 solar radii) of the upcoming Parker Solar Probe mission, $\beta_e \approx 0.01$, at least in fast-solar-wind streams (Chandran *et al.* 2011). Moreover, the growth-rate scaling (3.2) appears to be quite robust even at moderately large β_e : Numata & Loureiro (2015) showed that, keeping all other parameters fixed, $\gamma_{>} \propto \beta_e^{-1/2} \propto d_e$ up to at least $\beta_e = 10$, in agreement with (3.2), and despite the width of the reconnecting layer being set by ρ_e rather than d_e . Therefore, we expect our conclusions to be at least qualitatively relevant at $\beta_e \sim 1$.

4. Disruption scale

A sheet-like structure will be disrupted if its nonlinear cascade time (2.12) is longer than its disruption time (3.5). The disruption scale $\hat{\lambda}_{\text{D}}$ is then determined by demanding

$$\frac{\tau_{\text{C}}}{\tau_{\text{D}}} \sim \xi \frac{d_e \rho_s}{\lambda^3} \gtrsim 1. \quad (4.1)$$

Using (2.11) and (2.7), we find that, for n -th order aligned structures, this inequality is satisfied for

$$\hat{\lambda} \lesssim \hat{\lambda}_{\text{D}}[n] \sim \left(\frac{d_e \rho_s}{L_{\perp}^2} \right)^{\frac{2}{5}(1-2\zeta_n^{\perp}/5n)^{-1}}. \quad (4.2)$$

The scale $\hat{\lambda}_{\text{D}}$ is an increasing function of n . It is largest for the most intense structures, with $n \rightarrow \infty$, for which

$$\hat{\lambda}_{\text{D}}[\infty] \sim \left(\frac{d_e \rho_s}{L_{\perp}^2} \right)^{2/5}. \quad (4.3)$$

The scale at which the $n = 2$ structures, which determine the scaling of the second-order structure function and the energy spectrum, are disrupted is†

$$\hat{\lambda}_{\text{D}}[2] \sim \left(\frac{d_e \rho_s}{L_{\perp}^2} \right)^{4/9}, \quad (4.4)$$

‡ One can see that this is indeed what happens if, at the end of the nonlinear stage, the islands of width δ_{in} and length k_{tr}^{-1} circularise at constant area: their width after circularization is $w_{\text{circ}} \sim \sqrt{\delta_{\text{in}} k_{\text{tr}}^{-1}} \sim \lambda$.

† This scaling has also been independently derived by Loureiro & Boldyrev (2017b).

and, finally, the bulk fluctuations ($n \rightarrow 0$) are disrupted at

$$\hat{\lambda}_D[0] \sim \left(\frac{d_e \rho_s}{L_\perp^2} \right)^{0.46}. \quad (4.5)$$

The disruption may effectively be thought of as taking place over a narrow range of scales between $\hat{\lambda}_D[\infty]$ and $\hat{\lambda}_D[0]$, with $\hat{\lambda}_D[2]$ as a good representative. The disruption will only be relevant if any of these scales is larger than the scale at which the waves become dispersive, i.e.,

$$\begin{aligned} \frac{\lambda_D[n]}{\rho_s} &\sim \left(\frac{d_e}{\rho_s} \right)^{\frac{2}{5}(1-2\zeta_n^\perp/5n)^{-1}} \left(\frac{L_\perp}{\rho_s} \right)^{1-\frac{4}{5}(1-2\zeta_n^\perp/5n)^{-1}} \\ &\sim \left(\frac{m_i}{m_e} \frac{\beta_e}{Z} \right)^{-\frac{1}{5}(1-2\zeta_n^\perp/5n)^{-1}} \left(\frac{L_\perp}{\rho_s} \right)^{1-\frac{4}{5}(1-2\zeta_n^\perp/5n)^{-1}} \gtrsim 1. \end{aligned} \quad (4.6)$$

This gives us a critical β_e for structures at any given n to be disrupted:

$$\beta_e \lesssim \beta_e^{\text{crit}}[n] \sim Z \frac{m_e}{m_i} \left(\frac{L_\perp}{\rho_s} \right)^{1-2\zeta_n^\perp/n}. \quad (4.7)$$

For the $n = 2$ structures,

$$\beta_e^{\text{crit}}[2] \sim Z \frac{m_e}{m_i} \left(\frac{L_\perp}{\rho_s} \right)^{1/2}, \quad (4.8)$$

while for the most intense fluctuations ($n \rightarrow \infty$),

$$\beta_e^{\text{crit}}[\infty] \sim Z \frac{m_e}{m_i} \frac{L_\perp}{\rho_s}. \quad (4.9)$$

It is interesting to note that despite the fact that the dependence of $\hat{\lambda}_D[n]$ on n does not appear to be very strong [the exponents in (4.3), (4.4) and (4.5) are close together, at 0.40, 0.44, and 0.46 respectively], the dependence of β_e^{crit} on L_\perp/ρ_s is a strong function of n .

In the solar wind, typically $L_\perp/\rho_s \approx 10^3$ (Chen 2016), and so $\beta_e^{\text{crit}}[2] \sim 10^{-2}$, which is rare at 1AU but should be rather common closer to the Sun in the region to be explored by the Parker Solar Probe (Fox *et al.* 2016; Chandran *et al.* 2011). On the other hand, $\beta_e^{\text{crit}}[\infty] \sim 1$, and so one might expect the most intense sheet-like structures to become unstable to the onset of reconnection even at moderate β_e . Flux-rope-like ‘‘Alfvén vortex’’ structures extended in the parallel direction were indeed observed at ion scales in the solar wind by Perrone *et al.* (2016) and Lion *et al.* (2016). It is tempting to identify the structures produced by the disruption due to tearing with these observations†. We will study the structures produced by the disruption process in the next section, quantifying the relationship between their amplitude and scale, and further examining their importance as a function of β_e and of ρ_s/L_\perp .

Finally, let us set aside for a moment the precise values of β_e^{crit} for which we predict that disruption happens, and focus instead on the scaling of the break in the energy spectrum, $\hat{\lambda}_D[2]$, with physical parameters, i.e., the dependence of $\hat{\lambda}_D[2]$ on β . Chen *et al.* (2014)

† Cerri & Califano (2017) and Franci *et al.* (2017) observed reconnection onset and the formation of chains of multiple islands in their hybrid simulations of 2D kinetic turbulence. It is tempting to identify the island chains in their simulations with the structures that we predict here, but it should be noted that their simulations are 2D, and do not model electron inertia (or Ohmic resistivity), so the reconnection mechanism is quite different, and only a qualitative comparison can be made.

observed that at low β_i , the break scale of solar-wind turbulence appeared to scale as $d_i \propto \rho_i/\sqrt{\beta_i}$, in contradiction with expectations based on the linear physics of low- β plasmas (Schekochihin *et al.* 2009). Here we predict (ignoring the factor of $(L_\perp/\rho_s)^{1/9}$, which barely changes with the relevant physical parameters)

$$\frac{\lambda_D[2]}{\rho_s} \propto \beta_e^{-2/9} \quad \Rightarrow \quad \frac{\lambda_D[2]}{d_i} \propto \left(\beta_i \frac{T_e}{T_i} \right)^{5/18}. \quad (4.10)$$

For disruption due to reconnection to explain the anomalous break scale observed by Chen *et al.* (2014), there would therefore have to be correlations between β_i and T_e/T_i in their chosen intervals (namely, $T_i/T_e \propto \beta_i$ to match precisely). Encouragingly, in their data it does appear that the lower- β_i intervals are associated with markedly higher T_e/T_i .

5. Statistical properties of flux ropes

The dependence (4.2) of $\hat{\lambda}_D$ on n is one way of quantifying the scales at which the disrupted structures appear. In this section, we recast our calculation, treating the amplitude of the fluctuation as a random variable, i.e., we return to (2.2), and determine what fraction of the aligned structures remain undisrupted at any given scale, in terms of q (we remind the reader that this is an integer distributed as a Poisson random variable with mean $\langle q \rangle = \mu = -\ln \hat{\lambda}$). For a structure to be disrupted, we again demand (4.1) and, using (2.5), find that

$$\hat{\lambda}^{-5/2} A^q \frac{d_e \rho_s}{L_\perp^2} \gtrsim 1. \quad (5.1)$$

This is satisfied for

$$\begin{aligned} q \lesssim q_D &= \frac{(5/2) \ln \hat{\lambda} - \ln(d_e \rho_s / L_\perp^2)}{\ln A} \\ &= \frac{(5/2) \ln \hat{\lambda} - 2 \ln(\rho_s / L_\perp) + (1/2) \ln(\beta_e m_i / Z m_e)}{\ln A}. \end{aligned} \quad (5.2)$$

5.1. Filling factor of aligned turbulence

At any given scale, the filling factor of sheet-like, aligned structures that have not been affected by the disruption process (i.e., the probability of encountering them) is given by

$$f_0(\hat{\lambda}) = P(q > q_D) = 1 - \sum_{q=0}^{\lfloor q_D \rfloor} P(q), \quad (5.3)$$

where the distribution of q is given by (2.3). Similarly, the disruption causes a fractional reduction of energy contained in aligned sheet-like structures that is, using (2.4) and (2.2),

$$f_2(\hat{\lambda}) = 1 - \frac{1}{\langle \delta \hat{z}^2 \rangle} \sum_{q=0}^{\lfloor q_D \rfloor} \delta \hat{z}^2 P(q) = 1 - \frac{1}{\hat{\lambda}^{1/2}} \sum_{q=0}^{\lfloor q_D \rfloor} 2^{-q} P(q). \quad (5.4)$$

Obviously, (5.3) and (5.4) can only be considered quantitatively good estimates if f_0 and f_2 are close to unity, i.e., if the overall ‘‘RMHD ensemble’’ (described in Section 2) is not significantly altered.

Using (5.2), both f_0 and f_2 may be calculated numerically, as functions of $\hat{\lambda}$, ρ_s/L_\perp , and β_e . A particularly interesting case is $\lambda = \rho_s$, since this quantifies the cumulative effect of reconnection on the turbulence at the ion scale. Figure 1 shows the dependence

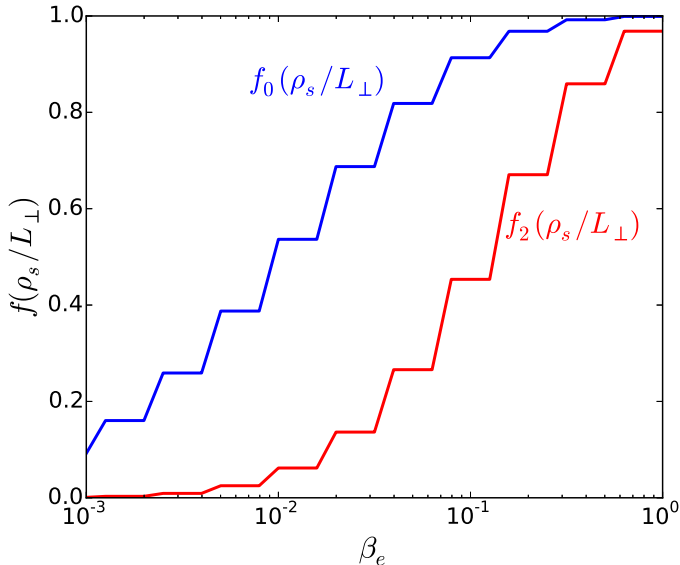


FIGURE 1. The filling factor of the aligned (i.e., undisrupted) structures at the ion sound scale $f_0(\rho_s/L_\perp)$ (blue) and fraction $f_2(\rho_s/L_\perp)$ of energy in them (red), plotted as a function of β_e . We have taken $\rho_s/L_\perp = 10^{-3}$, a reasonable value for the solar wind. Since q is an integer but q_D is not, the sums (5.3) and (5.4) are performed up to $\lfloor q_D \rfloor$, resulting in the discontinuities shown in the plot. In reality, of course, f_0 and f_2 will be smooth.

of $f_0(\rho_s/L_\perp)$ and $f_2(\rho_s/L_\perp)$ on β_e . The effect of disruption becomes more important at smaller β_e . Note that the amount of energy in the undisrupted structures at the ion scale is significantly reduced for values of β_e somewhat larger than $\beta_e^{\text{crit}}[2]$ given by (4.8). This suggests that, in practice, the turbulence is significantly affected by the disruption at only moderately small β_e : e.g., for $\beta_e \sim 0.1$, only around half of the energy that would be in sheets without disruption actually makes it to the ion scale, despite only around 10% by volume of the turbulence being disrupted.

5.2. Amplitude of flux ropes

We have proposed that the sheet-like structures with $q \sim q_D$ disrupted by tearing at the scale λ are converted into circular flux ropes, with perpendicular scale λ . We will assume that, just after they are created, they have the same amplitude as the sheet-like structure that produced them:

$$\delta \hat{z}_{\text{fr}} \sim \Lambda^{q_D}. \quad (5.5)$$

The flux ropes will not stay around for long: they will interact with each other and the remaining sheet-like structures, cascade, align, and form smaller, more sheet-like structures: this process will be studied in the next section. However, we can predict the relationship between the amplitude $\delta \hat{z}_{\text{fr}}$ and radius λ of the *newly created* flux ropes: upon inserting (5.2) into (5.5), we get

$$\delta \hat{z}_{\text{fr}} \sim \hat{\lambda}^{5/2} \left(\frac{L_\perp}{\rho_s} \right)^2 \left(\frac{\beta_e m_i}{Z m_e} \right)^{1/2}. \quad (5.6)$$

It is important to note that this is not a prediction for the scaling of any structure function or the spectrum of the disrupted turbulence (which will be worked out in the

next section); rather, this is a relationship describing *individual* flux ropes upon their formation within an aligned structure.

Thus, provided that β_e and ρ_s/L_\perp are small enough that $q_D > 0$ before the cascade reaches ρ_s , i.e., $\beta_e < \beta_e^{\text{crit}}[\infty]$ given by (4.9), there should be a strong relationship between the amplitude and radius of the structures at scales between $\hat{\lambda}_D[\infty]$, given by (4.3), and ρ_s : indeed, the scaling (5.6) is very steep with λ , and the flux ropes with the largest radius $\lambda_D[\infty]$ also have the largest amplitude, $\delta z_{\text{fr}} \sim \overline{\delta z}$. The scaling (5.6) could in principle be tested against observations such as those reported by Perrone *et al.* (2016), who observed 12 “Alfvén vortices” with diameters between $5\rho_i$ and $17\rho_i$ (as part of a sample of over 100 coherent structures of different types).

6. Disruption-range turbulence

In a realistic situation relevant to coronal or solar-wind turbulence, the separation between λ_D and ρ_s is so small that it would be challenging to establish a robust distinction between these two scales. It is nonetheless interesting to speculate on the nature of the turbulence in the interval $\lambda_D \gg \lambda \gg \rho_s$ in the asymptotic case where $L_\perp \rightarrow \infty$.

As described in Section 3, we expect the disruption process to convert the sheet-like structures just above λ_D into flux-rope-like structures just below λ_D . These are roughly circular in the perpendicular plane, with radius λ_D , but extended in the parallel direction due to critical balance. In order to treat this “disruption range” properly, we would need to account for the intermittency of both sheets and flux ropes. We do not attempt such a treatment in this paper. Instead, we develop a simpler model, in which we take the sheets and flux ropes to be effectively volume filling, and the sheets to have the properties of the $n = 2$ structures of Section 2 (since we would like to explore the scaling of the energy spectrum below λ_D). For simplicity of notation, we will drop the “[$n = 2$]” argument of all relevant quantities. A “characteristic fluctuation amplitude” $\delta z_{1,-}$ for the turbulence just below λ_D may be defined by assuming that there is negligible dissipation during the disruption process, so that the energy flux stays constant across the disruption scale[†]. Further assuming (radically) that the turbulence just below λ_D loses all its dynamic alignment, the scale ξ is no longer relevant and the only perpendicular scale in the

[†] The same assumption is made in the treatment of recursive disruptions in Section 6.1. This assumption may appear questionable (although, for a collisionless plasma, not necessarily impossible, since the reconnection itself is mediated by electron inertia and does not require dissipation), especially if the reconnection process were to proceed literally all the way to saturation, reconnecting all of the available flux and generating vigorous outflows, which can be Landau damped (Loureiro *et al.* 2013; TenBarge & Howes 2013; Bañón Navarro *et al.* 2016). Since the nonlinear cascade time, the linear tearing time, and the time for the islands to grow to the same width as the aligned structure that spawned them and thus disrupt it, are all of the same order, how much dissipation is likely to happen before this disruption may be a quantitative issue contingent on the precise, order-unity relationships between these times (note that Loureiro *et al.* 2013 report peak dissipation nearly 10 Alfvén times after peak reconnection). Boldyrev & Loureiro (2017) and Loureiro & Boldyrev (2017b) resolve this by assuming that the tearing mode can disrupt its mother sheet without needing to produce a perturbation of the magnetic field comparable in size to the fields associated with the sheet — and thus without dissipating much energy. We do not see how, dynamically, this can happen, since the process of disruption is presumably the very same nonlinear process that leads to islands perturbing the sheet finitely. Two further observations regarding dissipation in reconnection events are that (i) it is not necessarily the case that dissipation of energy caused during the disruption of a sheet of scale λ can be viewed as happening *at* scale λ , rather than as being part of the overall energy transfer towards smaller scales, where the dissipation actually occurs; (ii) how effective Landau damping is in dissipating energy in a truly collisionless, turbulent plasma is an open question (Schekochihin *et al.* 2016).

problem is λ_D :

$$\epsilon \sim \frac{\overline{\delta z}^3}{L_\perp} \sim \frac{\delta z_{1,-}^3}{\lambda_D}, \quad (6.1)$$

giving

$$\delta \hat{z}_{1,-} \sim \hat{\lambda}_D^{1/3}. \quad (6.2)$$

Note that this is smaller than the amplitude of the aligned turbulence at the same scale:

$$\delta \hat{z}_{1,+} \sim \hat{\lambda}_D^{1/4}. \quad (6.3)$$

The definition (6.2) might appear to be in contradiction with our earlier assumption (5.5) that the flux ropes should be formed with the same amplitude as their “mother sheet”. Indeed, if one took (5.5), (6.2) and (6.3) together, they imply that the flux ropes created by a disrupting sheet fill only a fraction of the mother sheet’s volume, contradicting our supposition above. However, (6.2) is not meant to be the amplitude of any individual structure, but rather an effective estimate that would on average give (6.1). In this sense, there is no difference between (6.2) or (6.3) and the usual “twiddle” relations in Kolmogorov-style turbulence phenomenologies relying on constant energy flux and ignoring intermittency and local imbalance: the amplitude (6.2) is an estimate that effectively absorbs within itself the filling fraction (probability of occurrence) of energetic structures that contribute to averages, as well as the (unknown) details of how precisely the nonlinear interactions within or between flux ropes (and between flux ropes and ambient turbulence) actually occur. In the case of flux ropes, it is clear that to make a connection between (5.5) and any average quantity, one would need to take into account the fact that they are clearly less volume-filling than their mother sheets, have shorter lifetimes, and might mainly cascade due to interactions between different types of structures. We leapfrog these issues with the aid of the requirement (6.1) that energy flux should stay the same. This will allow us to make progress and develop a simple model in this Section: (6.2) will define the “outer scale amplitude” for the Alfvénic cascade below λ_D . Intermittency is known to be of crucial importance in Alfvénic turbulence (Chandran *et al.* 2015; Mallet & Schekochihin 2017), and so a more rigorous model incorporating intermittency should be the subject of future work.

Following Mallet *et al.* (2017), the turbulence just below λ_D should behave just like the usual Alfvénic turbulence described in Section 2 (since $\lambda_D \gg \rho_s$): the flux ropes will interact with each other and the rest of the turbulence, causing a cascade to smaller scales[†]. In the course of this secondary cascade, the turbulence will again start to dynamically align and form sheet-like structures, and may eventually be disrupted by the onset of reconnection at a secondary disruption scale $\lambda_{D,2}$, at which the whole process repeats — provided that $\lambda_{D,2} > \rho_s$. Therefore, the turbulence between the first disruption scale λ_D (which we will now rechristen $\lambda_{D,1}$) and ρ_s is characterised by a sequence of disruptions, between which the turbulence re-aligns. We will now show that this recursive disruption process is unlikely to be fully realised, and usually terminates after only one disruption.

[†] The nonlinear evolution of the flux ropes is likely to be more complex than simply pairs of them merging into a single larger flux rope (Fermo *et al.* 2010). First, once the sheet is disrupted, the islands are not forced to stay at the location of the original sheet and so are not constrained to interact in a quasi-1D setting, moving along the sheet (cf. Uzdensky *et al.* 2010; Loureiro *et al.* 2012), or, indeed, to interact only with each other, rather than with the ambient turbulence. Secondly, since all this happens in three dimensions, they can cross, shear each other, or break up in more ways than are available to 2D plasmoids in a 1D sheet.

6.1. Recursive disruption?

The sequence of disruptions described above may be understood in terms of a recursion relation. After the $(i-1)$ st disruption, the turbulence undergoes the i th “mini-cascade”, with “outer-scale” values of the relevant quantities given by the values just below the $(i-1)$ st disruption scale $\lambda_{D,i-1}$:

$$\overline{\delta z} \rightarrow \delta z_{i-1,-}, \quad L_{\perp} \rightarrow \lambda_{D,i-1}. \quad (6.4)$$

Substituting this into (4.4) and normalising by L_{\perp} , we obtain the i -th disruption scale

$$\hat{\lambda}_{D,i} \sim \hat{\lambda}_{D,i-1}^{1/9} \left(\frac{d_e \rho_s}{L_{\perp}^2} \right)^{4/9} \sim \left(\frac{d_e \rho_s}{L_{\perp}^2} \right)^{\frac{1}{2} \left(1 - \frac{1}{9^i} \right)}. \quad (6.5)$$

Unlike in the resistive case (Mallet *et al.* 2017), this sequence will always terminate after a finite number of disruptions, because $\rho_s > d_e$ and so eventually $\lambda_{D,i} < \rho_s$. The number of disruptions is given by the greatest $i = i_{\max}$ for which

$$\frac{\lambda_{D,i}}{\rho_s} \sim \left(\frac{d_e}{\rho_s} \right)^{\frac{1}{2} \left(1 - \frac{1}{9^i} \right)} \left(\frac{L_{\perp}}{\rho_s} \right)^{\frac{1}{9^i}} > 1. \quad (6.6)$$

It is obvious from the exponent of L_{\perp}/ρ_s in (6.6) that, for there to be more than one disruption, L_{\perp}/ρ_s must be unrealistically large. Namely, (6.6) may be solved for i_{\max} , showing an extremely weak dependence on L_{\perp}/ρ_s :

$$i_{\max} = \frac{\ln \left[1 + \frac{2 \ln(L_{\perp}/\rho_s)}{\ln(\rho_s/d_e)} \right]}{2 \ln 3}. \quad (6.7)$$

With d_e/ρ_s kept constant as $L_{\perp}/\rho_s \rightarrow \infty$, the number of disruptions grows extremely slowly, so, in a moderately-low- β_e situation where $d_e/\rho_s < 1$, it is very unlikely that more than one disruption will occur.

6.2. Effective spectral index below λ_D : many disruptions

Nevertheless, in the spirit of asymptotic fantasising, let us determine the effective spectral index in a scale range featuring many disruptions. With the substitutions (6.4), the characteristic fluctuation amplitude just below each disruption scale is [cf. (6.2)]

$$\delta \hat{z}_{i,-} \sim \hat{\lambda}_{D,i}^{1/3}. \quad (6.8)$$

Therefore, the fluctuation amplitude associated with the i th aligning “mini-cascade” between disruption scales $\hat{\lambda}_{D,i-1}$ and $\hat{\lambda}_{D,i}$ is

$$\delta \hat{z}_i \sim \delta \hat{z}_{-,i-1} \left(\frac{\hat{\lambda}}{\hat{\lambda}_{D,i-1}} \right)^{1/4} \sim \hat{\lambda}_{D,i-1}^{1/3} \left(\frac{\hat{\lambda}}{\hat{\lambda}_{D,i-1}} \right)^{1/4}. \quad (6.9)$$

The characteristic aspect ratio of the turbulence (equivalently, the inverse alignment angle) between disruptions is then

$$\frac{\xi_i}{\lambda} \sim \left(\frac{\hat{\lambda}}{\hat{\lambda}_{D,i-1}} \right)^{-1/4}, \quad (6.10)$$

which is much smaller than the value $(\hat{\lambda}^{-1/4})$ that would have been attained without the disruptions. The “coarse-grained” fluctuation amplitude calculated at the scale just

above the i th disruption is [cf. (6.3)]

$$\delta \hat{z}_{i,+} \sim \hat{\lambda}_{D,i-1}^{1/3} \left(\frac{\hat{\lambda}_{D,i}}{\hat{\lambda}_{D,i-1}} \right)^{1/4} \sim \hat{\lambda}_{D,i} \left(\frac{d_e \rho_s}{L_\perp^2} \right)^{-1/3}, \quad (6.11)$$

where we have used (6.5) to obtain the second expression. Since (6.11) is larger than (6.8), our model spectrum looks like a sloping staircase, with (6.11) providing an upper envelope for the true scaling of the fluctuation amplitude (the true spectrum and structure function will not, of course, have discontinuities). Thus, $\delta z_{+,i} \propto \lambda_{D,i}$, and so the effective scaling exponent of the fluctuation amplitudes is $\alpha_{\text{eff}} = 1$. This implies a spectral index of $-1 - 2\alpha_{\text{eff}} = -3$, slightly steeper than the observed spectral index ≈ -2.8 below the ion scales in strong kinetic-Alfvén-wave turbulence in the solar wind (Alexandrova *et al.* 2009; Chen *et al.* 2010; Sahraoui *et al.* 2010).

Exactly the same scaling is (of course) found by observing that $\tau_C \sim \gamma_-^{-1}$ on the coarse-grained points $\hat{\lambda}_{D,i}$: then, constancy of energy flux through all scales implies that (cf. Boldyrev & Loureiro 2017)

$$\epsilon \sim \frac{\delta z_{i,+}^2}{\tau_C} \sim \gamma_- \delta z_{i,+}^2 \propto \frac{\delta z_{i,+}^3}{\lambda_{D,i}^3} \sim \text{const.} \quad \Rightarrow \quad \delta z_{+,i} \propto \lambda_{D,i}. \quad (6.12)$$

6.3. Effective spectral index below λ_D : one disruption

For realistic values of L_\perp and ρ_s , there is only one disruption, i.e., $i_{\text{max}} = 1$. The aligning cascade below λ_D then gives an amplitude at ρ_s of

$$\delta \hat{z}_{\rho_s} \sim \hat{\lambda}_D^{1/3} \left(\frac{\rho_s}{\lambda_D} \right)^{1/4}, \quad (6.13)$$

using (6.9). The characteristic aspect ratio of the turbulence at ρ_s is, using (6.10),

$$\frac{\xi_1}{\rho_s} \sim \left(\frac{\rho_s}{\lambda_D} \right)^{-1/4} \sim \left(\frac{m_i \beta_e}{m_e Z} \right)^{-1/18} \left(\frac{\rho_s}{L_\perp} \right)^{-1/36}, \quad (6.14)$$

which is approximately unity for any realistic set of parameters. Therefore, the turbulence at the ion scale, i.e., at the largest scales in the kinetic Alfvén wave cascade, will be very different depending on the presence or absence of the disruption: namely, it will either be nearly isotropic (in the perpendicular plane), as per (6.10), or highly anisotropic (aligned) with aspect ratio $(\rho_s/L_\perp)^{-1/4}$, respectively. In reality, there may be a mixture of both types of structures, as is suggested by the discussion in Section 5.1 — so the reduction in the alignment may not be as drastic as suggested by the extreme estimate (6.14).

The effective scaling of the fluctuation amplitudes between λ_D and ρ_s will be steeper than $\alpha_{\text{eff}} = 1$ derived in Section 6.2, because the recursive disruptions are cut off by the presence of the ion scale ρ_s . The effective scaling in this case is given by

$$\alpha_{\text{eff}} = \frac{\log(\delta \hat{z}_{1,+}/\delta \hat{z}_{\rho_s})}{\log(\lambda_D/\rho_s)}. \quad (6.15)$$

This ranges between $1 \leq \alpha_{\text{eff}} < \infty$, increasing the closer ρ_s gets to λ_D . Thus the effective spectral index in a “realistic” short range of scales between λ_D and ρ_s , with only one disruption, may be somewhat steeper than -3 , and may depend on β_e (i.e., it is not universal). Here again, the caveat that disruption does not in fact occur at a single scale or in every aligned structure implies that the spectrum should not be as dramatically steepened as (6.15) suggests. A spectrum slightly steeper than -3 is probably a reasonable expectation.

Short intervals of steep spectra are indeed sometimes observed near the ion scales in the solar wind: Sahraoui *et al.* (2010) and Lion *et al.* (2016) report a spectral index close to -4 in a small “transition range” of scales near the ion gyroradius. Lion *et al.* (2016) attribute this spectral index to Alfvén vortices (Alexandrova 2008) with scales a few times the ion gyroradius.

7. Discussion

Models of strong Alfvénic turbulence that incorporate dynamic alignment predict that the turbulent structures become progressively more sheet-like at smaller scales (Boldyrev 2006; Chandran *et al.* 2015; Mallet & Schekochihin 2017). This suggests that at some sufficiently small scale λ_D , the cascade time of the structures may be slower than the time required to disrupt them via magnetic reconnection. For resistive RMHD, this scale was calculated by Mallet *et al.* (2017) and Loureiro & Boldyrev (2017a). In this paper, we have extended this idea to the case of a weakly collisional, low- β_e plasma, in which the reconnection is due to electron inertia, rather than resistivity, and two-fluid effects become important at ion scales. We find that there is again a critical scale, $\hat{\lambda}_D \sim L_\perp^{1/9} (d_e \rho_s)^{4/9}$, below which the sheet-like structures are destroyed by reconnection. For sufficiently low electron beta, and sufficiently large scale separation between the outer scale L_\perp and the ion sound scale ρ_s , this scale lies in the inertial range: $\lambda_D > \rho_s$. The break in the energy spectrum of turbulence in a low- β collisionless plasma can thus occur at a larger scale than expected based on linear physics of wave modes — it does indeed do so in the solar wind (Bourouaine *et al.* 2012; Chen *et al.* 2014), although the observed scaling of the break scale with β_i appears to be stronger than we are able to predict here, unless there is some systematic correlation of the electron-ion temperature ratio with β_i .

We have argued that between λ_D and ρ_s , the spectral index of the turbulent fluctuations should be steeper than -3 . A steep “transition range” around the ion scale is indeed sometimes observed in the real solar wind (Sahraoui *et al.* 2010). This has been attributed to the presence of Alfvén vortices (Alexandrova 2008; Lion *et al.* 2016). These may be similar to the flux-rope-like structures that we envision in this paper to be the product of the disruption of the aligned cascade, and so disruption via tearing may be a physical reason for the presence of Alfvén vortices at ion scales in the solar wind. We predict that such structures should become very unlikely above a certain β_e [given by (4.9)], and that as β_e decreases, the proportion of the volume at the ion scale filled with aligned, undisrupted structures decreases, as does the amount of energy contained in them (Section 5.1). We also propose the relationship (5.6) between the amplitude and radius of the individual flux-rope structures. This could potentially be tested by solar-wind observations of the kind performed by Perrone *et al.* (2016).

For the Alfvénic turbulence to be disrupted by reconnection, we need $\lambda_D > \rho_s$. This inequality translates into a requirement that the electron plasma beta must be less than some critical value β_e^{crit} , given by (4.7), which depends on the ratio L_\perp/ρ_s of the outer scale to the ion scale and on the amplitude of the structures being considered. In the solar wind, $L_\perp/\rho_s \approx 10^3$, and we find that for fluctuations of moderate amplitude (ones that dominate the energy spectrum), $\beta_e^{\text{crit}} \sim 0.01$, while for the most intense (but rare and intermittent) fluctuations, $\beta_e^{\text{crit}} \sim 1$. Thus, we expect only the most intense structures to be disrupted in the solar wind at 1AU, where $\beta_e \sim 1$. Closer to the sun, β_e may be lower (Chandran *et al.* 2011), and the disruption process becomes more effective.

The turbulence at the ion scale is significantly different depending on whether disruption due to the onset of reconnection can occur or not. Above β_e^{crit} , sheet-like Alfvénic structures with a large aspect ratio will reach the ion scale without disruption. Below

β_e^{crit} , the disruption should occur, and turbulence at the ion scale should become much less anisotropic (less aligned) in the perpendicular plane (see Section 6.3). Thus, the nature of the turbulence at the ion scale, which provides the starting point for the sub-ion-scale kinetic-Alfvén-wave turbulence, depends crucially on whether the disruption process occurs.

Acknowledgements

We thank N. Loureiro and O. Alexandrova for useful conversations. The work of A.M. was supported by NSF grant AGS-1624501. B.D.G.C. was supported by NASA grants NNX15AI80G, NNX16AG81G, and NNX17AI18G, and NSF grant PHY-1500041. The work of A.A.S. was supported in part by grants from UK STFC and EPSRC.

Appendix A. Semicollisional disruption

Here, we will replicate some of the calculations done in the main text, but this time for a low- β “semicollisional”, large-guide-field regime where the width of the diffusive layer δ_{in} is smaller than ρ_s , but is controlled by resistivity rather than by electron inertia. For the turbulence, this means that the ion scale is greater than the resistive scale that would have provided the dissipative cutoff in fully collisional MHD,

$$\frac{\rho_s}{L_\perp} \gg S_{L_\perp}^{-3/4}, \quad (\text{A } 1)$$

but the electron-ion collision rate is nevertheless much larger than the nonlinear cascade rate of the fluctuations, or the growth rate of the tearing mode,

$$\nu_{ei} \gg \tau_C^{-1} \sim \gamma. \quad (\text{A } 2)$$

This means that the flux conservation is broken by Ohmic resistivity $\eta = \nu_{ei} d_e^2$ rather than by electron inertia, but the two-fluid effects are still important. This situation is relevant to many laboratory plasmas, for example TREX (Forest *et al.* 2015) and FLARE (Ji *et al.* 2014), as well as in hybrid-kinetic simulations that do not model the electron inertia (e.g., Parashar *et al.* 2009; Kunz *et al.* 2014; Cerri & Califano 2017; Cerri *et al.* 2017).

A.1. Semicollisional tearing mode

Growth rates of the tearing mode in this regime are reviewed in Appendix B.5 of Zocco & Schekochihin (2011). We will assume that the turbulent structures are still given by our RMHD turbulence model summarized in Section 2; viz., they have a width λ and length ξ in the perpendicular plane, and a perturbed-magnetic-field reversal $\delta b \sim \delta z$ across λ . The tearing mode in this regime, like its collisionless cousin in Section 3, involves three-scale physics: the (unstable) “equilibrium” at the scale of the turbulent structure λ , two-fluid effects at around the ion sound scale ρ_s , and flux unfreezing in an inner layer of width $\delta_{\text{in}} \ll \rho_s$, controlled by resistivity.

We will again consider the long-wavelength limit, $k\lambda \ll 1$, and assume (3.1). For $\Delta'\delta_{\text{in}} \ll 1$, the linear growth rate and the inner layer’s width are

$$\gamma_{>} \sim k\delta z (\Delta'\rho_s)^{2/3} (k\lambda S_\lambda)^{-1/3} \sim \frac{\delta z}{\lambda} \left(\frac{\rho_s}{\lambda}\right)^{2/3} S_\lambda^{-1/3}, \quad \delta_{\text{in}} \sim \lambda (\Delta'\rho_s)^{1/6} (k\lambda S_\lambda)^{-1/3}, \quad (\text{A } 3)$$

where $S_\lambda \doteq \delta z \lambda / \eta$ is the Lundquist number based on scale λ . Note that, as in the

collisionless case, $\gamma_>$ is independent of k . For $\Delta'\delta_{\text{in}} \sim 1$,

$$\gamma_< \sim k\delta z \left(\frac{\rho_s}{\lambda}\right)^{4/7} (k\lambda S_\lambda)^{-1/7}, \quad \delta_{\text{in}} \sim \lambda \left(\frac{\rho_s}{\lambda}\right)^{1/7} (k\lambda S_\lambda)^{-2/7}. \quad (\text{A } 4)$$

The transitional wavenumber k_{tr} between these two regimes may be found by balancing the two expressions for the growth rate, giving

$$k_{\text{tr}}\lambda \sim \left(\frac{\rho_s}{\lambda}\right)^{1/9} S_\lambda^{-2/9}. \quad (\text{A } 5)$$

For all $k > k_{\text{tr}}$, the growth rate is given by $\gamma_>$, so there is always a mode with the maximum growth rate that has a short enough wavelength to fit into the sheet.

The linear stage of tearing ends when the width of the islands reaches δ_{in} . This is largest for $k < k_{\text{tr}}$, so, at the end of the linear stage, the largest islands are again produced by the mode with $k \sim k_{\text{tr}}$, similarly to the collisionless case. We will, therefore, again assume that this mode dominates the nonlinear dynamics. We will also again assume that the X -points between the islands collapse on a timescale at least as short as the linear stage, and that the islands circularise forming a set of flux ropes. Similarly to the collisionless case, if they do so at constant area, their width is

$$w_{\text{circ}} \sim \sqrt{\delta_{\text{in}} k_{\text{tr}}^{-1}} \sim \lambda. \quad (\text{A } 6)$$

Since we are assuming that the circularisation is at least as fast as the linear stage, we can again estimate the disruption time using the linear growth rate (A 3),

$$\tau_{\text{D}} \sim \gamma_>^{-1}. \quad (\text{A } 7)$$

A.2. Disruption scale

Disruption of an aligned structure will occur if

$$\frac{\tau_{\text{C}}}{\tau_{\text{D}}} \sim \frac{\xi}{\lambda} \left(\frac{\rho_s}{\lambda}\right)^{2/3} S_\lambda^{-1/3} \gtrsim 1. \quad (\text{A } 8)$$

Therefore, the aligned structures are disrupted for

$$\hat{\lambda} < \hat{\lambda}_{\text{D}} \sim \left[\left(\frac{\rho_s}{L_\perp}\right)^2 S_{L_\perp}^{-1} \right]^{\frac{2}{9}(1-4\zeta_\perp^n/9n)^{-1}}. \quad (\text{A } 9)$$

For the $n = 2$ structures, this gives

$$\hat{\lambda}_{\text{D}}[2] \sim \left(\frac{\rho_s}{L_\perp}\right)^{1/2} S_{L_\perp}^{-1/4}, \quad (\text{A } 10)$$

while for the most intense structures ($n = \infty$),

$$\hat{\lambda}_{\text{D}}[\infty] \sim \left(\frac{\rho_s}{L_\perp}\right)^{4/9} S_{L_\perp}^{-2/9}. \quad (\text{A } 11)$$

The disruption scale is larger than ρ_s when S_{L_\perp} is below an n -dependent critical value:

$$S_{L_\perp} < S_{L_\perp}^{\text{crit}} \sim \left(\frac{L_\perp}{\rho_s}\right)^{\frac{5}{2}(1-4\zeta_n/5n)}. \quad (\text{A } 12)$$

For the $n = 2$ structures,

$$S_{L_\perp}^{\text{crit}}[2] \sim \left(\frac{L_\perp}{\rho_s}\right)^2, \quad (\text{A } 13)$$

and for the $n = \infty$ structures,

$$S_{L_\perp}^{\text{crit}}[\infty] \sim \left(\frac{L_\perp}{\rho_s} \right)^{5/2}. \quad (\text{A } 14)$$

Thus, the disruption becomes progressively more important to the aligned Alfvénic turbulence above the ion scale as S_{L_\perp} decreases — until $S_{L_\perp}^{-3/4} \gtrsim \rho_s/L_\perp$, at which point the semicollisional tearing mode scalings are no longer valid and the fully resistive regime studied in Mallet *et al.* (2017) is reached.

Note that, from (A 10),

$$\frac{\lambda_D[2]}{\rho_s} \sim \left(\frac{\rho_s}{L_\perp} \right)^{-1/2} S_{L_\perp}^{-1/4}. \quad (\text{A } 15)$$

This can be compared with attainable values of S_{L_\perp} and ρ_s/L_\perp in laboratory experiments: for example, according to Forest *et al.* (2015), the TREX experiment is able to access $10^3 \lesssim S_{L_\perp} \lesssim 10^5$ and $1 \lesssim L_\perp/\rho_s \lesssim 10^2$. This results in values of the disruption scale in the interval

$$2 \gtrsim \frac{\lambda_D[2]}{\rho_s} \gtrsim 0.1, \quad (\text{A } 16)$$

and so it is at least plausible that the disruption of Alfvénic turbulence by semicollisional tearing could be observed in such an experiment.

A.3. Amplitude of flux ropes

Instead of characterising the structures by n , we can, similarly to what we did with the collisionless case in Section 5, return to (2.2) and treat the amplitude of a fluctuation as a random variable. Via an analogous derivation, for disruption to occur, we must have

$$\frac{\tau_C}{\tau_D} \sim \frac{\xi}{\lambda} \left(\frac{\rho_s}{\lambda} \right)^{2/3} S_\lambda^{-1/3} \gtrsim 1 \quad \Rightarrow \quad \hat{\lambda}^{-3/2} \Lambda^{2q/3} \left(\frac{\rho_s}{L_\perp} \right)^{2/3} S_{L_\perp}^{-1/3} \gtrsim 1, \quad (\text{A } 17)$$

which is satisfied for

$$q \lesssim q_D = \frac{\ln \hat{\lambda} - (4/9) \ln(\rho_s/L_\perp) + (2/9) \ln S_{L_\perp}}{\ln \Lambda}. \quad (\text{A } 18)$$

One may use this and (2.3) to calculate the semicollisional versions of the filling fraction of aligned structures, f_0 , and the remaining fraction of their energy, f_2 [Section 5.1, (5.3) and (5.4), respectively], and show that as S_{L_\perp} decreases, these both become smaller.

If we again assume that the newly created flux ropes have the same amplitude as their mother sheets [see (5.5)], then, using (A 18), we obtain a relationship between δz_{fr} and λ of the flux ropes just after they are created:

$$\delta \hat{z}_{\text{fr}} \sim \hat{\lambda} \left(\frac{\rho_s}{L_\perp} \right)^{-4/9} S_{L_\perp}^{2/9}. \quad (\text{A } 19)$$

This relationship between the radii and amplitudes of individual flux ropes produced by the disruption of turbulent structures could in principle be tested in laboratory plasma devices, or in numerical simulations. Note that, as in Section 5.2, the largest flux ropes are produced with radius $\hat{\lambda}_D[n = \infty]$ and have amplitude $\delta z_{\text{fr}} \sim \overline{\delta z}$.

A.4. Recursive disruption?

Similarly to the collisionless case (Section 6), the flux-rope-like fluctuations just below the disruption scale should seed a new Alfvénic cascade to smaller scales, aligning, and

potentially disrupting again, and so on recursively until the ion scale ρ_s is reached. Let us again focus on $n = 2$, i.e., on the fluctuations that determine the scaling of the energy spectrum. Again, (6.2) and (6.4) describe the i th “mini-cascade”. The recursive relation between successive disruption scales is, analogously to (6.5):

$$\hat{\lambda}_{D,i} \sim \hat{\lambda}_{D,i-1}^{1/6} \left(\frac{\rho_s}{L_\perp} \right)^{1/2} S_{L_\perp}^{-1/4} \sim \left(\frac{\rho_s}{L_\perp} S_{L_\perp}^{-1/2} \right)^{\frac{3}{5}(1-\frac{1}{6^i})}. \quad (\text{A } 20)$$

This is valid for all i for which $\hat{\lambda}_{D,i} > \rho_s/L_\perp$, giving a condition for the i th disruption to be realised:

$$\frac{\lambda_{D,i}}{\rho_s} \sim \left(S_{L_\perp}^{3/4} \frac{\rho_s}{L_\perp} \right)^{-\frac{2}{5}(1-\frac{1}{6^i})} \left(\frac{L_\perp}{\rho_s} \right)^{\frac{1}{6^i}} \gtrsim 1. \quad (\text{A } 21)$$

This inequality is always violated for

$$i_{\max} \sim \frac{\ln \left(1 + \frac{5 \ln(L_\perp/\rho_s)}{2 \ln(S_{L_\perp}^{3/4} \rho_s/L_\perp)} \right)}{\ln 6} < \infty, \quad (\text{A } 22)$$

unless $\rho_s/L_\perp < S_{L_\perp}^{-3/4}$, at which point the semicollisional scalings are no longer valid and the system is in the fully resistive RMHD regime studied in Mallet *et al.* (2017). We again see that for there to be more than one disruption above ρ_s , L_\perp/ρ_s must be unrealistically large. Thus, the semicollisional regime, like the collisionless regime, is always characterised by a limited number of disruptions – usually a single disruption, for realistic parameters.

A.5. Effective spectral index below λ_D

Suppose, despite the arguments in the previous section as to the real-world irrelevance of this situation, that the range of scales between λ_D and ρ_s is asymptotically broad, and there are a large number of disruptions, $i_{\max} \gg 1$ (and also the semicollisional regime remains operative, i.e., $\rho_s/L_\perp > S_{L_\perp}^{-3/4}$). Using (6.4), the turbulent amplitude just below each disruption is again (6.8). Between successive disruption scales, the aligning cascade causes the turbulent amplitude to follow (6.9), and the aspect ratio of structures is given by (6.10), but now with the disruption scales $\hat{\lambda}_{D,i}$ given by (A 20). Again, the aspect ratio of the structures is greatly reduced by the disruption. The “coarse-grained” amplitudes calculated at the scales just above the i th disruption is [cf. (6.9)],

$$\delta \hat{z}_{i,+} \sim \hat{\lambda}_{D,i-1}^{1/3} \left(\frac{\hat{\lambda}_{D,i}}{\hat{\lambda}_{D,i-1}} \right)^{1/4} \sim \hat{\lambda}_{D,i}^{3/4} \left(\frac{\rho_s}{L_\perp} \right)^{1/4} S_{L_\perp}^{-1/8}. \quad (\text{A } 23)$$

Thus, in the semicollisional case, the effective scaling exponent of the fluctuation amplitude is $\alpha_{\text{eff}} = 3/4$, implying a spectral index of -2.5 . Exactly the same scaling is obtained by noticing that on the coarse-grained points $\hat{\lambda}_{D,i}$, the cascade time is just set by the linear growth rate of the tearing mode (A 3), $\tau_C \sim \gamma_{>}^{-1}$ and requiring that $\epsilon \sim \delta z^2/\tau_C \sim \text{const.}$ [cf. (6.12)].

For realistic values of ρ_s/L_\perp and S_{L_\perp} , there will be at most a single disruption before ρ_s . Essentially an identical argument to the one given in Section 6.3 implies that, due to the cutoff at ρ_s , the scaling of the fluctuation amplitudes may be nonuniversal, somewhat steeper than (A 23), and depend on the values of the physical parameters. As in the collisionless case, the presence of the disruption causes the structures at the ion scale to

be much less anisotropic within the perpendicular plane than they would have been had reconnection not interfered.

REFERENCES

- ALEXANDROVA, O. 2008 Solar wind vs. magnetosheath turbulence and Alfvén vortices. *Nonlin. Proc. Geophys.* **15**, 95.
- ALEXANDROVA, O., SAUR, J., LACOMBE, C., MANGENEY, A., MITCHELL, J., SCHWARTZ, S. J. & ROBERT, P. 2009 Universality of solar-wind turbulent spectrum from MHD to electron scales. *Phys. Rev. Lett.* **103**, 165003.
- BAÑÓN NAVARRO, A., TEACA, B., TOLD, D., GROSELJ, D., CRANDALL, P. & JENKO, F. 2016 Structure of plasma heating in gyrokinetic Alfvénic turbulence. *Phys. Rev. Lett.* **117**, 245101.
- BOLDYREV, S. 2006 Spectrum of magnetohydrodynamic turbulence. *Phys. Rev. Lett.* **96**, 115002.
- BOLDYREV, S. & LOUREIRO, N. F. 2017 Magnetohydrodynamic turbulence mediated by reconnection. *arXiv:1706.07139*.
- BOLDYREV, S. & PEREZ, J. C. 2012 Spectrum of kinetic-Alfvén turbulence. *Astrophys. J. Lett.* **758**, L44.
- BOUROUAINE, S., ALEXANDROVA, O., MARSCH, E. & MAKSIMOVIC, M. 2012 On Spectral Breaks in the Power Spectra of Magnetic Fluctuations in Fast Solar Wind between 0.3 and 0.9 AU. *Astrophys. J.* **749**, 102.
- BRUNO, R. & CARBONE, V. 2013 The solar wind as a turbulence laboratory. *Living Rev. Solar Phys.* **10**, 2.
- CERRI, S., FRANCI, L., CALIFANO, F., LANDI, S. & HELLINGER, P. 2017 Plasma turbulence at ion scales: a comparison between particle in cell and eulerian hybrid-kinetic approaches. *J. Plasma Phys.* **83**.
- CERRI, S. S. & CALIFANO, F. 2017 Reconnection and small-scale fields in 2D-3V hybrid-kinetic driven turbulence simulations. *New J. Phys.* **19**, 025007.
- CHANDRAN, B. D. G., DENNIS, T. J., QUATAERT, E. & BALE, S. D. 2011 Incorporating kinetic physics into a two-fluid solar-wind model with temperature anisotropy and low-frequency Alfvén-wave turbulence. *Astrophys. J.* **743**, 197.
- CHANDRAN, B. D. G., SCHEKOCHIHIN, A. A. & MALLET, A. 2015 Intermittency and alignment in strong RMHD turbulence. *Astrophys. J.* **807**, 39.
- CHANDRASEKHAR, S. 1961 *Hydrodynamic and Hydromagnetic Stability*. Oxford University Press.
- CHEN, C. H. K. 2016 Recent progress in astrophysical plasma turbulence from solar wind observations. *J. Plasma Phys.* **82**, 535820602.
- CHEN, C. H. K., BOLDYREV, S., XIA, Q. & PEREZ, J. C. 2013 Nature of subproton scale turbulence in the solar wind. *Phys. Rev. Lett.* **110**, 225002.
- CHEN, C. H. K., HORBURY, T. S., SCHEKOCHIHIN, A. A., WICKS, R. T., ALEXANDROVA, O. & MITCHELL, J. 2010 Anisotropy of solar wind turbulence between ion and electron scales. *Phys. Rev. Lett.* **104**, 255002.
- CHEN, C. H. K., LEUNG, L., BOLDYREV, S., MARUCA, B. A. & BALE, S. D. 2014 Ion-scale spectral break of solar wind turbulence at high and low beta. *Geophys. Res. Lett.* **41**, 8081–8088.
- CHEN, C. H. K., MALLET, A., SCHEKOCHIHIN, A. A., HORBURY, T. S., WICKS, R. T. & BALE, S. D. 2012 Three-dimensional structure of solar wind turbulence. *Astrophys. J.* **758**, 120.
- CHO, J. & LAZARIAN, A. 2004 The Anisotropy of Electron Magnetohydrodynamic Turbulence. *Astrophys. J.* **615**, L41.
- FERMO, R. L., DRAKE, J. F. & SWISDAK, M. 2010 A statistical model of magnetic islands in a current layer. *Phys. Plasmas* **17**, 010702.
- FOREST, C., FLANAGAN, K., BROOKHART, M., CLARK, M., COOPER, C., DSANGLES, V., EGEDAL, J., ENDRIZZI, D., KHALZOV, I., LI, H. & ET AL. 2015 The Wisconsin Plasma Astrophysics Laboratory. *J. Plasma Phys.* **81**, 345810501.
- FOX, N. J., VELLI, M. C., BALE, S. D., DECKER, R., DRIESMAN, A., HOWARD, R. A., KASPER, J. C., KINNISON, J., KUSTERER, M., LARIO, D., LOCKWOOD, M. K., MCCOMAS, D. J.,

- RAOUAFI, N. E. & SZABO, A. 2016 The Solar Probe Plus mission: humanity's first visit to our star. *Space Sci. Rev.* **204**, 7.
- FRANCI, L., CERRI, S. S., CALIFANO, F., LANDI, S., PAPINI, E., VERDINI, A., MATTEINI, L., JENKO, F. & HELLINGER, P. 2017 Magnetic reconnection as a driver for a sub-ion scale cascade in plasma turbulence. *ArXiv e-prints*, arXiv: 1707.06548.
- GOLDREICH, P. & SRIDHAR, S. 1995 Toward a theory of interstellar turbulence. 2: Strong alfvénic turbulence. *Astrophys. J.* **438**, 763.
- GOLDREICH, P. & SRIDHAR, S. 1997 Magnetohydrodynamic turbulence revisited. *Astrophys. J.* **485**, 680.
- GRECO, A., PERRI, S., SERVIDIO, S., YORDANOVA, E. & VELTRI, P. 2016 The complex structure of magnetic field discontinuities in the turbulent solar wind. *Astrophys. J. Lett.* **823**, L39.
- HARRIS, E. G. 1962 On a plasma sheath separating regions of oppositely directed magnetic field. *Nuovo Cimento* **23** (1), 115–121.
- Ji, H., BHATTACHARJEE, A., PRAGER, S., DAUGHTON, W. S., BALE, S. D., CARTER, T. A., CROCKER, N., DRAKE, J. F., EGEDAL, J., SARFF, J., WALLACE, J., BELOVA, E., ELLIS, R., FOX, II, W. R., HEITZENROEDER, P., KALISH, M., JARA-ALMONTE, J., MYERS, C. E., QUE, W., REN, Y., TITUS, P., YAMADA, M. & YOO, J. 2014 FLARE (Facility for Laboratory Reconnection Experiments): A major next step for laboratory studies of magnetic reconnection. *AGU Fall Meeting Abstracts*.
- KADOMTSEV, B. & POGUTSE, O. 1973 Nonlinear helical perturbations of a plasma in the tokamak. *Soviet Phys. JETP* **38**, 283.
- KUNZ, M. W., SCHEKOCHIHIN, A. A. & STONE, J. M. 2014 Firehose and mirror instabilities in a collisionless shearing plasma. *Phys. Rev. Lett.* **112**, 205003.
- LION, S., ALEXANDROVA, O. & ZASLAVSKY, A. 2016 Coherent events and spectral shape at ion kinetic scales in the fast solar wind turbulence. *Astrophys. J.* **824**, 47.
- LOUREIRO, N. F. & BOLDYREV, S. 2017a Role of magnetic reconnection in MHD turbulence. *Phys. Rev. Lett.* **118**, 245101.
- LOUREIRO, N. F. & BOLDYREV, S. 2017b Collisionless reconnection in magnetohydrodynamic and kinetic turbulence. *ArXiv e-prints*, arXiv: 1707.05899.
- LOUREIRO, N. F., SAMTANEY, R., SCHEKOCHIHIN, A. A. & UZDENSKY, D. A. 2012 Magnetic reconnection and stochastic plasmoid chains in high-Lundquist-number plasmas. *Phys. Plasmas* **19**, 042303.
- LOUREIRO, N. F., SCHEKOCHIHIN, A. A. & ZOCCO, A. 2013 Fast collisionless reconnection and electron heating in strongly magnetized Plasmas. *Phys. Rev. Lett.* **111**, 025002.
- MALLET, A. & SCHEKOCHIHIN, A. A. 2017 A statistical model of three-dimensional anisotropy and intermittency in strong alfvénic turbulence. *Mon. Not. R. Astron. Soc.* **466**, 3918.
- MALLET, A., SCHEKOCHIHIN, A. A. & CHANDRAN, B. D. G. 2015 Refined critical balance in strong Alfvénic turbulence. *Mon. Not. R. Astron. Soc.* **449**, L77.
- MALLET, A., SCHEKOCHIHIN, A. A. & CHANDRAN, B. D. G. 2017 Disruption of sheet-like structures in Alfvénic turbulence by magnetic reconnection. *Mon. Not. R. Astron. Soc.* **468**, 4862.
- MALLET, A., SCHEKOCHIHIN, A. A., CHANDRAN, B. D. G., CHEN, C. H. K., HORBURY, T. S., WICKS, R. T. & GREENAN, C. C. 2016 Measures of three-dimensional anisotropy and intermittency in strong Alfvénic turbulence. *Mon. Not. R. Astron. Soc.* **459**, 2130.
- MASON, J., CATTANEO, F. & BOLDYREV, S. 2006 Dynamic alignment in driven magnetohydrodynamic turbulence. *Phys. Rev. Lett.* **97**, 255002.
- MATTHAEUS, W. H. & LAMKIN, S. L. 1986 Turbulent magnetic reconnection. *Phys. Fluids* **29**, 2513.
- NUMATA, R. & LOUREIRO, N. F. 2015 Ion and electron heating during magnetic reconnection in weakly collisional plasmas. *J. Plasma Phys.* **81**, 305810201.
- OSMAN, K. T., MATTHAEUS, W. H., GOSLING, J. T., GRECO, A., SERVIDIO, S., HNAT, B., CHAPMAN, S. C. & PHAN, T. D. 2014 Magnetic reconnection and intermittent turbulence in the solar wind. *Phys. Rev. Lett.* **112**, 215002.
- PARASHAR, T., SHAY, M., CASSAK, P. & MATTHAEUS, W. 2009 Kinetic dissipation and anisotropic heating in a turbulent collisionless plasma. *Phys. Plasmas* **16**, 032310.

- PÉREZ, J. C., MASON, J., BOLDYREV, S. & CATTANEO, F. 2012 On the Energy Spectrum of Strong Magnetohydrodynamic Turbulence. *Phys. Rev. X* **2**, 041005.
- PERRONE, D., ALEXANDROVA, O., MANGENEY, A., MAKSIMOVIC, M., LACOMBE, C., RAKOTO, V., KASPER, J. C. & JOVANOVIĆ, D. 2016 Compressive coherent structures at ion scales in the slow solar wind. *Astrophys. J.* **826**, 196.
- POLITANO, H., POUQUET, A. & SULEM, P. L. 1989 Inertial ranges and resistive instabilities in two-dimensional magnetohydrodynamic turbulence. *Phys. Fluids B* **1**, 2330.
- RETINÒ, A., SUNDKVIST, D., VAIVADS, A., MOZER, F., ANDRÉ, M. & OWEN, C. 2007 In situ evidence of magnetic reconnection in turbulent plasma. *Nature Phys.* **3**, 236.
- SAHRAOUI, F., GOLDSTEIN, M. L., BELMONT, G., CANU, P. & REZEAU, L. 2010 Three dimensional anisotropic k spectra of turbulence at subproton scales in the solar wind. *Phys. Rev. Lett.* **105**, 131101.
- SCHEKOCHIHIN, A. A., COWLEY, S. C., DORLAND, W., HAMMETT, G. W., HOWES, G. G., QUATAERT, E. & TATSUNO, T. 2009 Astrophysical gyrokinetics: kinetic and fluid turbulent cascades in magnetized weakly collisional plasmas. *Astrophys. J. Supp.* **182**, 310.
- SCHEKOCHIHIN, A. A., PARKER, J. T., HIGHCOCK, E. G., DELLAR, P. J., DORLAND, W. & HAMMETT, G. W. 2016 Phase mixing versus nonlinear advection in drift-kinetic plasma turbulence. *J. Plasma Phys.* **82**, 905820212.
- SERVIDIO, S., MATTHAEUS, W. H., SHAY, M. A., CASSAK, P. A. & DMITRUK, P. 2009 Magnetic reconnection in two-dimensional magnetohydrodynamic turbulence. *Phys. Rev. Lett.* **102**, 115003.
- STRAUSS, H. R. 1976 Nonlinear, three-dimensional magnetohydrodynamics of noncircular tokamaks. *Phys. Fluids* **19**, 134.
- SUNDKVIST, D., RETINÒ, A., VAIVADS, A. & BALE, S. D. 2007 Dissipation in turbulent plasma due to reconnection in thin current sheets. *Phys. Rev. Lett.* **99**, 025004.
- TENBARGE, J. M. & HOWES, G. G. 2012 Evidence of critical balance in kinetic Alfvén wave turbulence simulations. *Phys. Plasmas* **19**, 055901.
- TENBARGE, J. M. & HOWES, G. G. 2013 Current sheets and collisionless damping in kinetic plasma turbulence. *ApJ* **771**, L27.
- UZDENSKY, D. A., LOUREIRO, N. F. & SCHEKOCHIHIN, A. A. 2010 Fast magnetic reconnection in the plasmoid-dominated regime. *Phys. Rev. Lett.* **105**, 235002.
- VERDINI, A. & GRAPPIN, R. 2015 Imprints of expansion on the local anisotropy of solar wind turbulence. *Astrophys. J. Lett.* **808**, L34.
- WICKS, R. T., MALLET, A., HORBURY, T. S., CHEN, C. H. K., SCHEKOCHIHIN, A. A. & MITCHELL, J. J. 2013 Alignment and Scaling of Large-Scale Fluctuations in the Solar Wind. *Phys. Rev. Lett.* **110**, 025003.
- ZHDANKIN, V., BOLDYREV, S. & UZDENSKY, D. A. 2016 Scalings of intermittent structures in magnetohydrodynamic turbulence. *Phys. Plasmas* **23** (5), 055705.
- ZHDANKIN, V., UZDENSKY, D. A., PÉREZ, J. C. & BOLDYREV, S. 2013 Statistical analysis of current sheets in three-dimensional magnetohydrodynamic turbulence. *Astrophys. J.* **771**, 124.
- ZOCCO, A. & SCHEKOCHIHIN, A. A. 2011 Reduced fluid-kinetic equations for low-frequency dynamics, magnetic reconnection, and electron heating in low-beta plasmas. *Phys. Plasmas* **18**, 102309.